Variations in stratospheric inorganic chlorine between 1991 and 2006

D. J. Lary,[1,2] D. W. Waugh,[3] A. R. Douglass,[2] R. S. Stolarski,[2] P. A. Newman,[2] and H. Mussa[4]

Received 16 March 2007; revised 28 August 2007; accepted 21 September 2007; published 13 November 2007.

[1] A consistent time series of stratospheric inorganic chlorine Cl_y from 1991 to present is formed using spaceborne observations together with neural networks. A neural network is first used to account for inter-instrument biases in HCl observations. A second neural network is used to learn the abundance of Cl_y as a function of HCl and CH_4, and to form a time series using available HCl and CH_4 measurements. The estimates of Cl_y are broadly consistent with calculations based on tracer fractional releases and previous estimates of stratospheric age of air. These new estimates of Cl_y provide a critical test for global models, which exhibit significant differences in predicted Cl_y and ozone recovery. **Citation:** Lary, D. J., D. W. Waugh, A. R. Douglass, R. S. Stolarski, P. A. Newman, and H. Mussa (2007), Variations in stratospheric inorganic chlorine between 1991 and 2006, *Geophys. Res. Lett.*, *34*, L21811, doi:10.1029/2007GL030053.

1. Introduction

[2] Knowledge of the distribution of inorganic chlorine Cl_y in the stratosphere is needed to attribute changes in stratospheric ozone to changes in halogens, and to assess the realism of chemistry-climate models [*Eyring et al.*, 2006; *Eyring et al.*, 2007]. However, there are limited direct observations of Cl_y. Simultaneous measurements of the major inorganic chlorine species are rare [*Zander et al.*, 1992; *Gunson et al.*, 1994; *Bonne et al.*, 2000; *Nassar et al.*, 2006]. In the upper stratosphere, Cl_y can be inferred from HCl alone [e.g., *Anderson et al.*, 2000; *Froidevaux et al.*, 2006b].

[3] Here we combine observations from several spaceborne instruments using neural networks [*Lary and Mussa*, 2004] to produce a time series for Cl_y. A neural network is used to characterize differences among various HCl measurements, and to perform an inter-instrument bias correction. Measurements from several different instruments are used in this analysis. These instruments, together with temporal coverage and measurement uncertainties, are listed in Table 1. The HALOE uncertainties are only estimates of random error and do not include any indications of overall accuracy. All instruments provide measurements through the depth of the stratosphere. A second neural network is used to infer Cl_y from these corrected HCl measurements and measurements of CH_4.

[4] Sections 2 and 3 describe the HCl and Cl_y intercomparisons. Section 4 presents a summary.

2. HCl Intercomparison

[5] We first compare measurements of HCl from the different instruments listed in Table 1. Comparisons are made in equivalent PV latitude - potential temperature coordinates [*Schoeberl et al.*, 1989; *Proffitt et al.*, 1989; *Lait et al.*, 1990; *Douglass et al.*, 1990; *Lary et al.*, 1995; *Schoeberl et al.*, 2000] to extend the effective latitudinal coverage of the measurements and identify contemporaneous measurements in similar air masses.

[6] The Halogen Occultation Experiment (HALOE) provides the longest record of space based HCl observations. Figure 1 compares HALOE HCl with HCl observations from (1) the Atmospheric Trace Molecule Spectroscopy Experiment (ATMOS), (2) the Atmospheric Chemistry Experiment (ACE), and (3) the Microwave Limb Sounder (MLS). In these plots each point is the median HCl observation made by the instrument during each month for 30 equivalent latitude bins from pole to pole and 25 potential temperature bins from the 300–2500 K potential temperature surfaces.

[7] For each of these bins we only use data in the range where the supplied quality flags show it suitable for scientific use. For each bin, we characterize the median observation uncertainty and the representativeness uncertainty. The representativeness is a measure of the spatial variability over the bin, in our case characterized by the average deviation of the observations in the bin. The average deviation is a measure of the width of the probability distribution of observations. Unlike the standard deviation, the average deviation is not strongly influenced by a few outliers. Each of these uncertainties are used later in Figures 2 and 3.

[8] A consistent picture is seen in these plots: HALOE HCl measurements are lower than those from the other instruments. The slopes of the linear fits (relative scaling) are 1.05 for the HALOE-ATMOS comparison, 1.09 for the HALOE-MLS, and 1.18 for the HALOE-ACE. The offsets are apparent at the 525 K isentropic surface and above. Previous comparisons among HCl datasets reveal a similar bias for HALOE [*Russell et al.*, 1996; *McHugh et al.*, 2005; *Froidevaux et al.*, 2006a]. ACE and MLS HCl measurements are in much better agreement (Figure 1d). Note, all measurements agree within the stated observational uncertainties summarized in Table 1.

[9] To combine the above HCl measurements to form a continuous time series of HCl (and then Cl_y) from 1991 to 2006 it is necessary to account for the biases between data

[1]Goddard Earth Sciences and Technology Center, University of Maryland Baltimore County, Baltimore, Maryland, USA.
[2]Atmospheric Chemistry and Dynamics Branch, NASA Goddard Space Flight Center, Greenbelt, Maryland, USA.
[3]Department of Earth and Planetary Sciences, Johns Hopkins University, Baltimore, Maryland, USA.
[4]Department of Chemistry, University of Cambridge, Cambridge, UK.

Copyright 2007 by the American Geophysical Union.
0094-8276/07/2007GL030053

Table 1. Instruments and Constituents Used in Constructing the Cl_y Record From 1991–2006[a]

Instrument	Temporal Coverage	Species	References	Median Observation Uncertainty
ACE v2.2	2004–2006	HCl, $ClONO_2$ ClO, and HOCl	[*Bernath et al.*, 2005]	8% (HCl), 30% ($ClONO_2$) >100% (ClO), >100% (HOCl)
ATMOS	1991, 1993, 1994	HCl, $ClONO_2$	[*Zander et al.*, 1992]	8% (HCl), 60% ($ClONO_2$)
Aura MLS v1	2004–2006	HCl, ClO and HOCl	[*Froidevaux et al.*, 2006a]	12% (HCl), 76% (ClO), >100% (HOCl)
CLAES v9	1991–1993	$ClONO_2$	[*Roche et al.*, 1993]	>100%
CRISTA	1994, 1997	$ClONO_2$	[*Offermann et al.*, 1999]	61%
HALOE v19	1991–2005	HCl	[*Russell et al.*, 1993]	4%
UARS MLS v5	1991–1999	ClO	[*Waters et al.*, 1996]	>100% (ClO)

[a]The uncertainties given are the median values calculated for each level 2 measurement profile and its uncertainty (both in mixing ratio) for all the observations made. The uncertainties are larger than usually quoted for MLS ClO because they reflect the single profile precision, which is improved by temporal and/or spatial averaging. The HALOE uncertainties are only estimates of random error and do not include any indications of overall accuracy.

sets. A neural network is used to learn the mapping from one set of measurements onto another as a function of equivalent latitude and potential temperature [*Lary and Mussa*, 2004]. We consider two cases. In one case ACE HCl is taken as the reference and the HALOE and Aura HCl observations are adjusted to agree with ACE HCl. In the other case HALOE HCl is taken as the reference and the Aura and ACE HCl observations are adjusted to agree with HALOE HCl. In both cases we use equivalent latitude and potential temperature to produce average profiles. The purpose of the mapping is simply to learn the bias as a function of location, not to imply which instrument is correct.

[10] The precision of the correction using the neural network mapping is of the order of ≈0.3 ppbv, as seen in Figure 1e which shows the results when HALOE HCl measurements have been mapped into ACE measurements. The mapping has removed the bias between the measurements and has also straightened out the 'wiggles' in Figure 1c, i.e., the neural network has learned the equivalent PV latitude and potential temperature dependence of the bias between HALOE and MLS. The inter-instrument offsets are not constant in space or time, and are not a simple function of Cl_y.

3. Inorganic Chlorine Cl_y

[11] To a first approximation $Cl_y \approx HCl + ClONO_2 + ClO + HOCl$ [*Brasseur and Solomon*, 1987]. However, observations of $ClONO_2$, ClO and HOCl are much more limited than those of HCl (for example, there is no ACE ClO product available above 29.5 km). As shown in Table 1, $ClONO_2$ measurements have been made by CLAES (1991–1993), ATMOS (1992–1994), CRISTA (1994, 1998), and ACE (2004–present). ClO measurements have been made by the UARS MLS (1991–1999), aircraft, MkIV, ACE, and Aura MLS (2004–present). HOCl measurements have been made by ACE and Aura MLS.

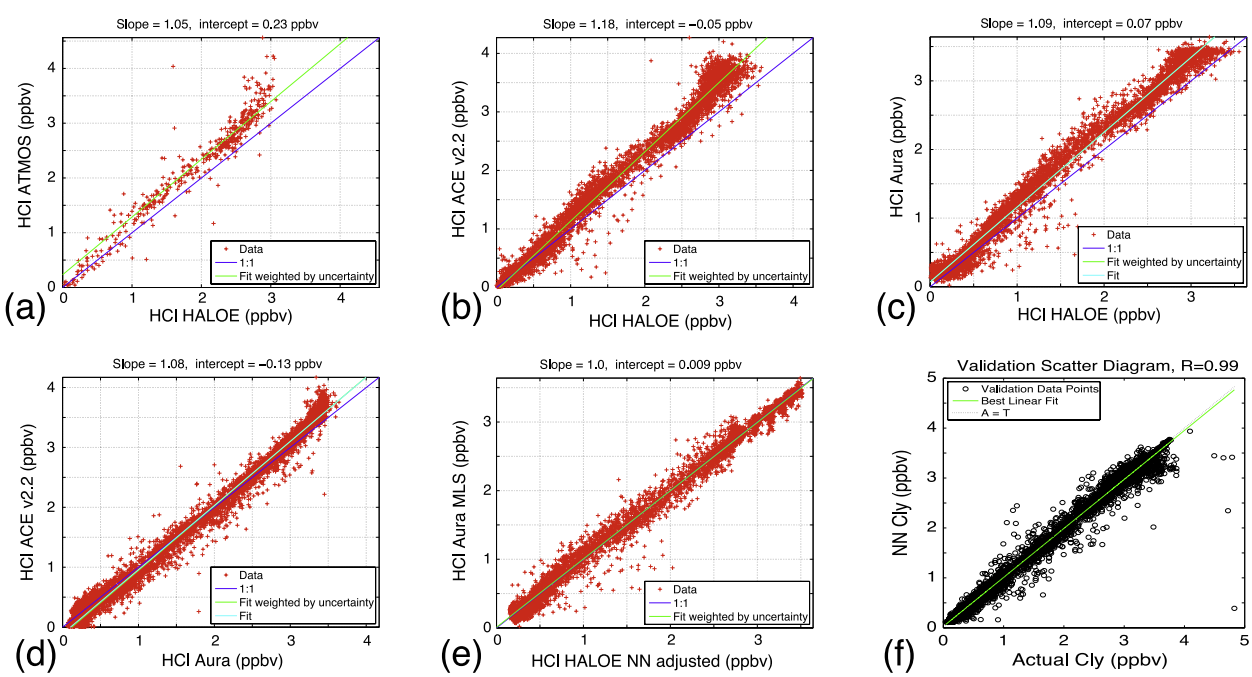

Figure 1. (a, b, c, d) Scatter plots of all contemporaneous observations of HCl made by HALOE, ATMOS, ACE, and MLS Aura. In Figure s 1a, 1b, and 1c HALOE is shown on the x-axis. (e) As in Figure 1c except that it uses the neural network 'adjusted' HALOE HCl values. (f) The validation scatter diagram of the neural network estimate of $Cl_y \approx HCl + ClONO_2 + ClO + HOCl$ versus the actual Cl_y for a totally independent data sample not used in training the neural network.

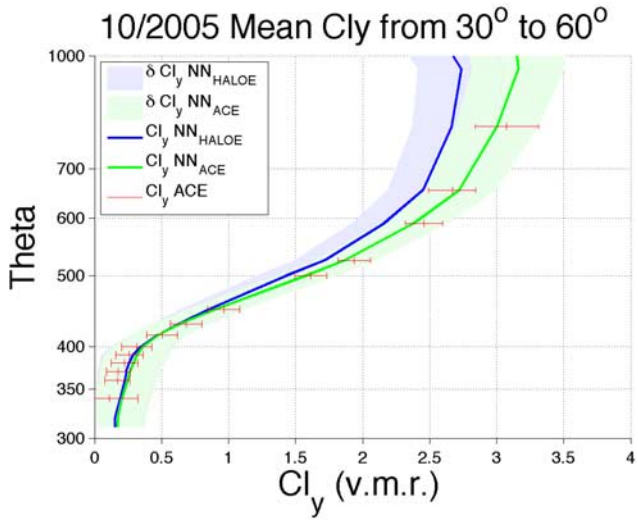

Figure 2. Cl_y average profiles between 30° and 60°N for October 2005, estimated by neural network calibrated to HALOE HCl (blue curve), estimated by neural network calibrated to ACE HCl (green), or from ACE observations of HCl, ClONO2, ClO, and HOCl (red crosses). In each case, the shaded range represents the total uncertainty; it includes the observational uncertainty, the representativeness uncertainty (the variability over the analysis grid cell), and the neural network uncertainty. The vertical extent of this plot was limited to below 1000 K (≈35 km), as there is no ACE v2.2 ClO data for the upper altitudes. In addition, above ≈750 K (≈25 km) ClO constitutes a larger fraction of Cl_y (up to about 10%) and so the large uncertainties in ClO have greater effect.

[12] Because of the limited temporal coverage of $ClONO_2$ measurements it is not possible to form a continuous time series of Cl_y by combining HCl, $ClONO_2$, HOCl, and ClO. However, it is possible to form a time series of Cl_y using a neural network trained by the available Cl_y observations. There are sufficient observations of $ClONO_2$, ClO and HOCl from aircraft, ACE, ATMOS, CLAES, CRISTA, MkIV and MLS to train a neural network to learn the Cl_y abundance as a function of HCl and CH_4, for each of which there is a long, near-continuous, time series of measurements. The resulting reconstruction reproduces an independent validation dataset faithfully with a correlation coefficient of 0.99, and provides a scatter diagram with a slope very close to one for the observed Cl_y plotted against the neural network inferred Cl_y, see Figure 1f.

[13] The inputs to the neural network that estimates Cl_y are HCl, CH_4, equivalent latitude and potential temperature. HCl is used because it is continuously observed from the launch of UARS to the present and is typically the major Cl_y reservoir. CH_4 is used because it is continuously observed from the launch of UARS to the present and, as a long-lived tracer, it is well correlated with Cl_y. Potential temperature and equivalent latitude are used because the correlation between long-lived tracers such as CH_4 and Cl_y is a strong function of altitude and a weak function of latitude [*Lary and Mussa*, 2004]. When we do the training we randomly split our training dataset into three portions of 80%, 10% and 10%. The 80% is used to train the neural network weights. This training is iterative and on each iteration we evaluate the current RMS error of the neural network. The RMS error is calculated by using the second 10% of the data that was not used in the training. We use the RMS error and the way it changes with training iteration (epoch) to determine the convergence of our training. When the training is complete, we use the final 10% as a validation dataset. This 10% of the data was randomly chosen and not used in either the training or RMS evaluation. We only use the neural network if the validation scatter diagram, which plots the actual data from validation portion against the neural network estimate, yields a straight line graph with a slope of 1. This is a stringent and independent validation. The validation is global as the data was randomly selected

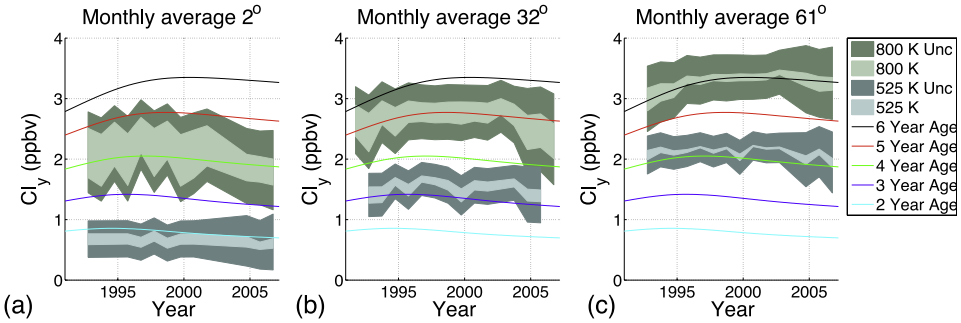

Figure 3. (a, b, c) October Cl_y time-series for the 525 K isentropic surface (≈20 km) and the 800 K isentropic surface (≈30 km). In each case the dark shaded range represents the total uncertainty in our estimate of Cl_y. This total uncertainty includes the observational uncertainty, the representativeness uncertainty (the variability over the analysis grid cell), the inter-instrument bias in HCl, the uncertainty associated with the neural network inter-instrument correction, and the uncertainty associated with the neural network inference of Cl_y from HCl and CH_4. The inner light shading depicts the uncertainty on Cl_y due to the inter-instrument bias in HCl alone. The upper limit of the light shaded range corresponds to the estimate of Cl_y based on all the HCl observations calibrated by a neural network to agree with ACE v2.2 HCl. The lower limit of the light shaded range corresponds to the estimate of Cl_y based on all the HCl observations calibrated to agree with HALOE v19 HCl. Overlaid are lines showing the Cl_y based on age of air calculations [*Newman et al.*, 2006]. To minimize variations due to differing data, coverage months with less than 100 observations of HCl in the equivalent latitude bin were left out of the time-series.

over all temporal and spatial data points available. Several training strategies were examined, the one described included the most species over the longest time period.

[14] Figure 2 shows how Cl_y profiles estimated by the neural network agree directly with observed Cl_y for October 2005. In each case the shaded range represents the total uncertainty associated with the Cl_y estimate. The HCl bias between HALOE and ACE (the difference between the green and blue lines) is a major uncertainty. To enable us to compare these neural network fits to observations, the red crosses with error bars show the observed $Cl_y \approx HCl + ClONO_2 + ClO + HOCl$ based on the available ACE data, and there is good agreement between these observations and the neural network calibrated to ACE data (note ACE ClO is not available above 30 km).

[15] The distribution of Cl_y is expected to change between 1991 and 2006 as the abundances of its source gases have changed. Figure 3 shows the time-series of Cl_y for the 525 K isentropic surface (≈20 km) and the 800 K isentropic surface (≈30 km), for three different equivalent latitudes. The upper limit of each light shaded range corresponds to the estimate of Cl_y for the neural network calibrated to agree with ACE v2.2 HCl, and the lower limit to the estimate of Cl_y for the neural network calibrated to agree with HALOE v19 HCl. The dark shading in Figure 3 shows the total uncertainty, the root mean square of the observational uncertainty, the representativeness uncertainty (the variability over the analysis grid cell PV-theta bin), the inter-instrument bias in HCl, the uncertainty associated with the neural network inter-instrument correction, and the uncertainty associated with the neural network inference of Cl_y from HCl and CH_4. We estimate the uncertainty due to the neural network fitting using the neural network validation scatter diagram. This scatter diagram shows a cloud of finite width about the 1:1 line. We use the width of the cloud as an estimate of the uncertainty associated with the neural network fitting.

[16] The variation in Cl_y estimates between the two cases depends on latitude, altitude and season and is typically $\leq$0.4 ppbv at 800 K. There is a general tendency of Cl_y to increase in the 1990s, peak around 2000, and then slowly decrease. This is consistent with our expectations based on the tropospheric abundance of chlorine containing source gases. The Cl_y time-series shown in Figure 3 constitutes a useful test for model simulations. The variation in simulated Cl_y from the chemistry-climate models used in the recent [*World Meteorological Organization* (*WMO*), 2006] report is much greater than the above uncertainty in Cl_y. For example, the simulated peak annual-mean Cl_y for north mid-latitudes varies from 0.8 to 2.8 ppb [*Eyring et al.*, 2007]. We have represented this uncertainty by the light shading.

[17] The estimates of Cl_y produced are broadly consistent with calculations based on tracer fractional releases [*Newman et al.*, 2006] and previous estimates of stratospheric age of air. Observations show that at 20 km the mean age increases from around 2 years in the tropics to around 4 years at high latitudes (60°N), with a similar gradient at 30 km but older ages by around 2 years [*Waugh and Hall*, 2002]. The curves in Figure 3 show calculations of Cl_y for a range of values of the mean age of air, and the ages that are required to match the observed Cl_y are consistent with the observations of the mean age.

4. Summary

[18] A consistent time series of stratospheric Cl_y from 1991 to present has been formed using available spaceborne observations. Here we used neural networks to intercalibrate HCl measurements from different instruments, and to estimate Cl_y from observations of HCl and CH_4. These estimates of Cl_y peaked in the late 1990s and have begun to decline as expected from tropospheric measurements of source gases and troposphere to stratosphere transport times. Furthermore, the estimates of Cl_y are consistent with calculations based on tracer fractional releases and age of air [*Newman et al.*, 2006]. The Cl_y time-series formed here is an important benchmark for models being used to simulate the recovery of the ozone hole. Although there is uncertainty in the estimates of Cl_y, primarily due to biases in HCl measurements, this uncertainty is small compared with the range of model predictions shown in the recent [*WMO*, 2006] report.

[19] **Acknowledgments.** It is a pleasure to acknowledge NASA for research funding (Aura Validation and MAP), Lucien Froidevaux and the Aura MLS team for their data, the ACE team, Peter Bernath, Chris Boone, and Kaley Walker for their data, the HALOE team and Ellis Remsberg for their data, and the ATMOS team for their data. The ACE mission is funded primarily by the Canadian Space Agency.

References

Anderson, J., J. M. Russell, S. Solomon, and L. E. Deaver (2000), Halogen Occultation Experiment confirmation of stratospheric chlorine decreases in accordance with the Montreal protocol, *J. Geophys. Res.*, *105*(D4), 4483–4490.

Bernath, P. F., et al. (2005), Atmospheric Chemistry Experiment (ACE): Mission overview, *Geophys. Res. Lett.*, *32*, L15S01, doi:10.1029/2005GL022386.

Bonne, G. P., et al. (2000), An examination of the inorganic chlorine budget in the lower stratosphere, *J. Geophys. Res.*, *105*(D2), 1957–1971.

Brasseur, G., and S. Solomon (1987), *Aeronomy of the Middle Atmosphere: Chemistry and Physics of the Stratosphere and Mesosphere*, *Atmos. Sci. Libr.*, 2nd ed., D. Reidel, Norwell, Mass.

Douglass, A., R. Rood, R. Stolarski, M. Schoeberl, M. Proffitt, J. Margitan, M. Loewenstein, J. Podolske, and S. Strahan (1990), Global 3-dimensional constituent fields derived from profile data, *Geophys. Res. Lett.*, *17*, 525–528.

Eyring, V., et al. (2006), Assessment of temperature, trace species, and ozone in chemistry-climate model simulations of the recent past, *J. Geophys. Res.*, *111*, D22308, doi:10.1029/2006JD007327.

Eyring, V., et al. (2007), Multi-model projections of stratospheric ozone in the 21st century, *J. Geophys. Res.*, *112*, D16303, doi:10.1029/2006JD008332.

Froidevaux, L., et al. (2006a), Early validation analyses of atmospheric profiles from EOS MLS on the aura satellite, *IEEE Trans. Geosci. Remote Sens.*, *44*(5), 1106–1121.

Froidevaux, L., et al. (2006b), Temporal decrease in upper atmospheric chlorine, *Geophys. Res. Lett.*, *33*, L23812, doi:10.1029/2006GL027600.

Gunson, M. R., M. C. Abrams, L. L. Lowes, E. Mahieu, R. Zander, C. P. Rinsland, M. K. W. Ko, N. D. Sze, and D. K. Weisenstein (1994), Increase in levels of stratospheric chlorine and fluorine loading between 1985 and 1992, *Geophys. Res. Lett.*, *21*, 2223–2226.

Lait, L., et al. (1990), Reconstruction of O_3 and N_2O fields from ER-2, DC-8, and balloon observations, *Geophys. Res. Lett.*, *17*, 521–524.

Lary, D. J., and H. Y. Mussa (2004), Using an extended Kalman filter learning algorithm for feed-forward neural networks to describe tracer correlations, *Atmos. Chem. Phys. Discuss.*, *4*, 3653–3667.

Lary, D., M. Chipperfield, J. Pyle, W. Norton, and L. Riishojgaard (1995), 3-dimensional tracer initialization and general diagnostics using equivalent PV latitude-potential-temperature coordinates, *Q. J. R. Meteorol. Soc.*, *121*, 187–210.

McHugh, M., B. Magill, K. A. Walker, C. D. Boone, P. F. Bernath, and M. Russell III (2005), Comparison of atmospheric retrievals from ACE

and HALOE, *Geophys. Res. Lett.*, *32*, L15S10, doi:10.1029/2005GL022403.

Nassar, R., et al. (2006), A global inventory of stratospheric chlorine in 2004, *J. Geophys. Res.*, *111*, D22312, doi:10.1029/2006JD007073.

Newman, P. A., E. R. Nash, S. R. Kawa, S. A. Montzka, and S. M. Schauffler (2006), When will the Antarctic ozone hole recover?, *Geophys. Res. Lett.*, *33*, L12814, doi:10.1029/2005GL025232.

Offermann, D., K. U. Grossmann, P. Barthol, P. Knieling, M. Riese, and R. Trant (1999), Cryogenic Infrared Spectrometers and Telescopes for the Atmosphere (CRISTA) experiment and middle atmosphere variability, *J. Geophys. Res.*, *104*(D13), 16,311–16,325.

Proffitt, M., M. J. Steinkamp, J. A. Powell, R. J. McLaughlin, O. A. Mills, A. L. Schmeltekopf, T. L. Thompson, A. F. Tuck, T. Tyler, and K. R. Chan (1989), In situ ozone measurements within the 1987 Antarctic ozone hole from a high-altitude ER-2 aircraft, *J. Geophys. Res.*, *94*(D14), 16,547–16,555.

Roche, A. E., J. B. Kumer, J. L. Mergenthaler, G. A. Ely, W. G. Uplinger, J. F. Potter, T. C. James, and L. W. Sterritt (1993), The Cryogenic Limb Array Etalon Spectrometer (CLAES) on UARS: Experiment description and performance, *J. Geophys. Res.*, *98*(D6), 10,763–10,775.

Russell, J. M., III, L. L. Gordley, J. H. Park, S. R. Drayson, W. D. Hesketh, R. J. Cicerone, A. F. Tuck, J. E. Frederick, J. E. Harries, and P. J. Crutzen (1993), The Halogen Occultation Experiment, *J. Geophys. Res.*, *98*(D6), 10,777–10,797.

Russell, J. M., III, et al. (1996), Validation of hydrogen chloride measurements made by the Halogen Occultation Experiment from the UARS platform, *J. Geophys. Res.*, *101*(D6), 10,151–10,162.

Schoeberl, M. R., L. R. Lait, P. A. Newman, R. L. Martin, M. H. Profitt, D. L. Hartmann, M. Lowenstein, J. Podolske, S. E. Strahan, and B. Gary (1989), Reconstruction of the constituent distribution and trends in the Antarctic polar vortex from ER-2 flight observations, *J. Geophys. Res.*, *94*(D14), 16,815–16,845.

Schoeberl, M. R., L. C. Sparling, C. H. Jackman, and E. L. Fleming (2000), A Lagrangian view of stratospheric trace gas distributions, *J. Geophys. Res.*, *105*(D1), 1537–1552.

Waters, J. W., et al. (1996), Validation of UARS Microwave Limb Sounder ClO measurements, *J. Geophys. Res.*, *101*(D6), 10,091–10,127.

Waugh, D., and T. Hall (2002), Age of stratospheric air: Theory, observations, and models, *Rev. Geophys.*, *40*(4), 1010, doi:10.1029/2000RG000101.

World Meteorological Organization (WMO) (2006), Scientific assessment of ozone depletion: 2006, *Tech. Rep. 50*, WMO Global Ozone Res. and Monit. Proj., Geneva, Switzerland.

Zander, R., M. R. Gunson, C. B. Farmer, C. P. Rinsland, F. W. Irion, and E. Mahieu (1992), The 1985 chlorine and fluorine inventories in the stratosphere based on ATMOS observations at 30-degrees north latitude, *J. Atmos. Chem.*, *15*(2), 171–186.

A. R. Douglass, P. A. Newman, and R. S. Stolarski, Atmospheric Chemistry and Dynamics Branch, NASA Goddard Space Flight Center, Greenbelt, MD 20771, USA.

D. J. Lary, Goddard Earth Sciences and Technology Center, University of Maryland Baltimore County, Baltimore, MD 21228, USA. (david@lary.umbc.edu)

H. Mussa, Department of Chemistry, University of Cambridge, Lensfield Road, Cambridge CB2 1EW, UK.

D. W. Waugh, Department of Earth and Planetary Sciences, Johns Hopkins University, 320 Olin Hall, 3400 N. Charles Street, Baltimore, MD 21218, USA.